INTERNATIONAL JOURNAL FOR NUMERICAL METHODS IN FLUIDS, VOL. 19, 575–603 (1994)

A NUMERICAL APPROACH TO MODEL NON-ISOTHERMAL VISCOUS FLOW THROUGH FIBROUS MEDIA WITH FREE SURFACES

M. V. BRUSCHKE AND S. G. ADVANI

Department of Mechanical Engineering, University of Delaware, Newark, DE, U.S.A.

SUMMARY

A numerical simulation is presented to predict the free surface and its interactions with heat transfer and cure for flow of a shear-thinning resin through the fibre preform. the flow part of the simulation is based on the finite element/control volume method. Since the traditional control volume approach produces an error associated with a mass balance inconsistency, a new method which overcomes this issue is proposed, the element control volume method.

The heat transfer and cure analysis in the simulation are based on the finite difference/control volume method. Since heat conduction is dominant in the through-thickness direction and most of the heat convection is in-plane, heat transfer and cure are solved in fully three-dimensional form. A simple concept of the boundary condition constant is introduced which models a realistic mould configuration with a heating element located at a distance behind the mould wall. The varying viscosity throughout the mould associated with the strain rate, temperature and degree of cure distribution may be accounted for in calculating the mould-filling pattern. This introduces a two-way coupling between momentum and energy transport in fibrous media during mould filling.

KEY WORDS Resin transfer moulding Porous media Composites processing Finite element/control volume Heat transfer Cure

1. INTRODUCTION

Flow through porous media has long been a topic of particular interest to fields such as petroleum engineering and ground-water hydrology. The medium through which the flow takes place is generally granular and relatively isotropic. Porous media made up of fibers introduce an added complexity in that, depending on the fibre arrangement, the media may become highly anisotropic. For example, a medium made up of aligned fibres may have a resistance to flow in the fibre direction which is an order of magnitude different from the resistance perpendicular to the fibre direction.[1,2] Flow through fibrous media is of interest in such fields as filtration and composites manufacturing. One such manufacturing process is resin transfer moulding (RTM), which takes place under non-isothermal circumstances. That is, the fluid, the mould and the fibres may have different temperatures and the temperature will vary throughout the porous medium. In addition, the fluids used may be non-Newtonian and the viscosity may change not only with the shear rate but also with temperature and degree of cure.

In general the RTM process consists of four phases.[3–5] A schematic view of the process steps is shown in Figure 1. The first phase, *preform lay-up*, encompasses the cutting of one or more pieces of fibre mat or continuous fibre strands into specified shapes. The pieces are then stacked and placed in the mould in desired orientations. The second phase, *mould filling*, begins when

CCC 0271–2091/94/190575–29

Received 2 October 1992
Revised 24 March 1994

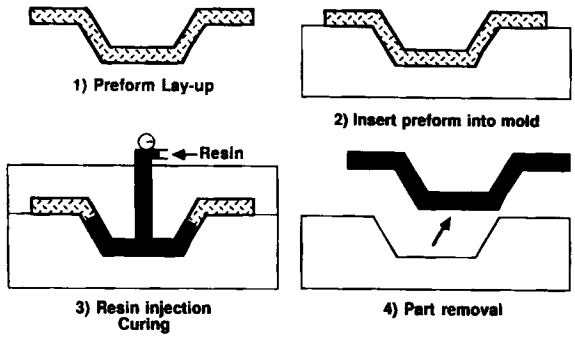

Figure 1. RTM process steps

the mould is closed and viscous fluid is injected into the hot mould. The fluid is usually a thermoset polymeric resin and flows around and through the fibre network until the mould is filled. Vents should ideally be located at the points of the mould which fill last, to allow the displaced air to escape. Heat transfer during this phase predominantly results from conduction from the mould walls to the fluid and the flow will be non-isothermal. In the case of high-speed processes such as structural resin injection molding (SRIM), viscous dissipation may also play a role in the heat transfer. Once the mould is full, the phase of *curing* starts. The cure is initiated by the heat transfer from the hot mould to the cold resin and the polymer reacts into a cross-linked network while releasing heat. During this reaction the fluid viscosity increases exponentially to infinity as the fluid solidifies. Ideally the curing reaction should not begin until the mould is completely filled, since the solidification of the resin may prevent it from impregnating the total fibre preform. The curing reaction is highly exothermic and will therefore affect the heat transfer substantially. The final phase, *part removal*, takes place after the curing reaction is complete and the part has solidified. A mould release agent is usually applied to the mould for easy removal of the part.

The mould-filling pattern for flow of a fluid through the fibre preform depends on a number of parameters. The part geometry, the location of the injection gates and the injection pressures or flow rates are perhaps the most obvious ones. RTM parts are typically thin shell non-planar structures, the thickness being much less than the other overall dimensions of the part. Multiple gates may be used to inject the fluid into the part and injection can take place by regulating the flow rate or the injection pressure. Another parameter which will influence the mould-filling pattern is the structure of the fibre preform. Fibre preform with different geometries or fibre arrangements will offer a different resistance to the flow. Last, the fluid viscosity will vary throughout the mould as a function of temperature, degree of cure and, since most resins are shear-thinning, as a function of the strain rate. To successfully predict the mould-filling behaviour, all these parameters and the nature of coupling should be correctly represented.

The numerical techniques used to predict mould filling should incorporate the coupling between heat transfer, resin cure and flow. In this paper we present a simulation to predict the free surface, heat transfer and cure for flow of a resin through the fibre preform. Since RTM parts are typically thin shell non-planar parts, only the in-plane flow is considered. The finite element method is used to solve for the pressure distribution throughout the mould. The moving free surface flow front is treated using the control volume method. The traditional control volume method produces an error associated with a mass balance inconsistency. A modified control volume approach which eliminates this type of error has been developed. The heat transfer and

cure are treated using a three-dimensional finite difference method. It is essential to solve for the temperature in three dimensions, since although most of the heat is convected in the plane of the part, the dominant mode of heat conduction is in the thickness direction, from the hot mould wall to the cold resin. In porous media dispersion of heat may also be important if the Peclet number is large.[6] We assume that dispersion does not contribute to the energy equation. However, the results from the heat transfer part of the simulation are still coupled with the flow simulation to predict the mould filling accurately.

2. THEORY

Flow through porous media has traditionally been described by the empirical Darcy law,[7] which relates the fluid flow rate to the pressure gradient, fluid viscosity and permeability of the porous medium:

$$\bar{v} = -\frac{K}{\eta}\frac{\Delta P}{L}, \tag{1}$$

in which $\bar{v}$ is the superficial velocity, the velocity one observes on a macroscopic scale; η is the viscosity of the fluid, $\Delta P/L$ is the pressure gradient in the direction of flow over a characteristic dimension of L, and K is the permeability of the porous medium. The permeability is a measure of the ease of flow through the medium and is a function of the structure and porosity of the medium.

Most mould-filling processes in anisotropic porous media deals with parts which have a shell-like geometry, the thickness being much smaller than the other dimensions of the part. This allows us to ignore the flow in the thickness direction and model the flow locally as two-dimensional. The fibrous preform is treated as an incompressible porous medium and a two-dimensional version of Darcy's law is used to describe the pressure–flow rate relationship in a medium with non-isotropic permeability.[8] In using a two-dimensional form of Darcy's law, we give up the details of the velocity profile through the thickness and use average velocities. These gap-wise averaged velocities $\bar{v}$ for an isothermal generalized Newtonian fluid may be written in matrix form as

$$\begin{pmatrix}\bar{u}_x\\ \bar{u}_y\end{pmatrix} = -\frac{1}{\eta_{\text{eff}}}\begin{pmatrix}K_{xx} & K_{xy}\\ K_{yx} & K_{yy}\end{pmatrix}\begin{pmatrix}\partial P/\partial x\\ \partial P/\partial y\end{pmatrix}. \tag{2}$$

Here η_{eff} is the viscosity of the fluid, P is the pressure and K is the permeability tensor, which is a second-order tensor. In the case of shear-thinning fluids the viscosity is also a function of the pressure gradient and the resulting equations are non-linear.[1,9] Other variables which may influence the effective viscosity are the local temperature and the degree of cure.[5]

Even if the permeability of the anisotropic porous medium does change in magnitude, as long as its principal directions remain the same, one can always diagonalize the permeability matrix. Usually the reinforcement and hence the permeability matrix will vary throughout the mould. The reinforcement will consist of different types of mats or lay-ups placed at different orientations in the mould. For such cases it is not possible to find a common principal co-ordinate system in which the permeability matrix wil diagonalize everywhere in the mould. Hence one has to take into account the full permeability matrix. After applying the continuity condition to Equation (2), the governing equation for the pressure distribution becomes

$$\frac{\partial}{\partial x}\left(\frac{K_{xx}}{\eta_{\text{eff}}}\frac{\partial P}{\partial x}\right) + \frac{\partial}{\partial x}\left(\frac{K_{xy}}{\eta_{\text{eff}}}\frac{\partial P}{\partial y}\right) + \frac{\partial}{\partial y}\left(\frac{K_{yx}}{\eta_{\text{eff}}}\frac{\partial P}{\partial x}\right) + \frac{\partial}{\partial y}\left(\frac{K_{yy}}{\eta_{\text{eff}}}\frac{\partial P}{\partial y}\right) = 0, \tag{3}$$

where the value of the permeability matrix may vary throughout the mould.

The boundary conditions on equation (3) are zero pressure at the free flow front and, since we assume there is no leakage through the mould walls, the velocity component normal to the mould wall has to equal zero at the mould wall. For an isotropic porous medium this results in zero pressure gradient normal to the mould boundary. However, for an anisotropic medium we have

$$\bar{u}_n = -\frac{1}{\eta_{\text{eff}}}\left(K_{nn}\frac{\partial P}{\partial n} + K_{nt}\frac{\partial P}{\partial t}\right) = 0, \tag{4}$$

where n denotes the direction normal to the mould wall and t the direction tangent to the mould wall. Once the pressure distribution has been found, averaged velocities across the thickness can be calculated from equation (2).

This pressure formulation is presently widely used,[9–13] since it enables one to solve for a scalar variable rather than for a vectorial quantity such as the velocity. The advantage is that one can solve the governing equation for non-planar shell-like geometries in three-dimensional space.

2.1. Heat transfer and cure

In processes such as RTM the mould filling does not take place under isothermal conditions. In general the mould is heated and cool resin is injected into the mould. As the resin flows through the fibre preform, heat transfer between the mould walls, the fibre preform and the resin will take place. Therefore the resin temperature will vary thoughout the mould. Since the fluid viscosity is strongly dependent on the temperature, it will also vary throughout the mould, thus influencing the mould-filling pattern. Moreover, as the resin temperature increases, cure will initiate. Resin cure is a strongly exothermic reaction which will influence the overall heat transfer substantially.

A simple scaling analysis reveals that heat conduction in the thickness direction from the mould wall to the resin is as important as convection in the in-plane flow direction. Consequently, it is not possible to limit the analysis to the thin shell approach adopted for the flow simulation. The heat transfer needs to be analysed in three dimensions to account for the energy balance of conduction in the thickness direction, convection in the in-plane directions and heat generation due to the exothermic reaction when curing initiates. Once the temperature field is known, the fluid viscosities may be calculated. A through-thickness average fluid viscosity may then be used to solve for the pressure distribution.

2.1.1. Energy equation. Heat transfer in flow through porous media has been analysed by a variety of authors.[14–17] It should be noted that no universal agreement exists on the analysis of the heat transfer in porous media. Several authors have presented studies of heat transfer during composite manufacturing processes, using a number of different approaches.[18–20] The approaches can be grouped into two categories: the two-phase models and the equilibrium models. In the two-phase model one takes into account convection between the fibre preform and the fluid. However, no theoretical means of predicting the heat transfer coefficient governing this convection process exists and thus it has to be determined experimentally for each fluid/fibre preform combination. The equilibrium approach assumes the fluid and fibre medium to have the same temperature at each point. In essence, one assumes the heat transfer coefficient to be infinite. An experimental study[19,21] on flow through fibre mats has shown that the equilibrium model is a valid assumption in slow processes such as RTM. For the heat transfer in a fast

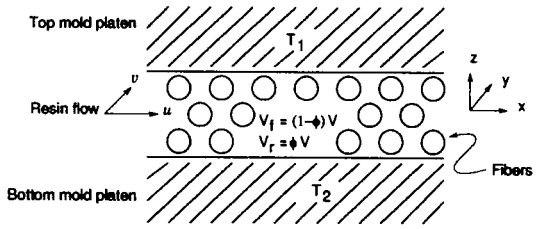

Figure 2. Cross-subsection of a mould with fluid and fibre preform

process such as SRIM, this assumption may break down. Here the equilibrium model will be used to account for the heat transfer between the fibres and the fluid.

The constituents in the mould are resin and fibre preforms as depicted in Figure 2, so the intrinsic thermodynamic quantity internal energy will represent both. Since we are considering a thin shell geometry, for which the thickness is small compared with the other dimensions, a scaling analysis will show that the in-plane conduction and out-of-plane convection are negligible and can therefore be ignored. Ignoring convection in the thickness direction is also consistent with the method used to solve for the movement of the free surface flow front. For RTM flows the Peclet number is usually low, hence we assume that the heat dispersion effect due to the pores in insignificant. With these assumptions the energy equation takes the form

$$[\phi\rho_r c_{p_r} + (1-\phi)\rho_f c_{p_f}]\frac{\partial T}{\partial t} + \phi\rho_r c_{p_r}\left(\bar{u}_x\frac{\partial T}{\partial x} + \bar{u}_y\frac{\partial T}{\partial y}\right) = \kappa\frac{\partial^2 T}{\partial z^2} + \phi\dot{s}, \tag{5}$$

where T is the temperature, t is the time, ρ_r, c_{p_r}, ρ_f and c_{p_f} are the density and heat capacity of the resin and fibre preform respectively and ϕ is the porosity or $1 - V_f$, where V_f is the fibre volume fraction. The first term represents the change in internal energy of both the fluid and the fibre preform. The second term represents the contribution due to convection of the fluid. Conduction through the thickness is taken into account by the first term on the right-hand side, $\dot{s}$ is the source term and represents the energy generated in the resin as a result of curing. Normally this term is very small or should be small until the filling is complete. Since the filling time is much shorter than the reaction time in RTM, this term does not pose any numerical problems, κ is the effective through-thickness conductivity of the fluid/fibre medium combination, which may be calculated using a self-consistent model.[22] The self-consistent model is based on a simplification of the medium consisting of cylinders. Using this model, the effective conductivity for a transversely isotropic fibre medium and fluid may be expressed in terms of the conductivity of the fibrous medium, κ_f, and that of the fluid or resin, κ_r, as

$$\kappa = \kappa_f\frac{(\kappa_f + \kappa_r) + (\kappa_f - \kappa_r)(1-\phi)}{(\kappa_f + \kappa_r) - (\kappa_f - \kappa_r)(1-\phi)}. \tag{6}$$

To solve for Equation (5), four boundary conditions need to be applied. At the boundaries of the physical domain three conditions are necessary, one each at the top and bottom mould platens and one at the flow front. Since in-plane conduction is ignored, no boundary condition is necessary at the mould side edges. Finally, a boundary condition is needed at the injection gates.

Several types of boundary conditions (constant temperature, convective or mixed) may be applied to the temperature equation at the top and bottom mould platens. The simplest

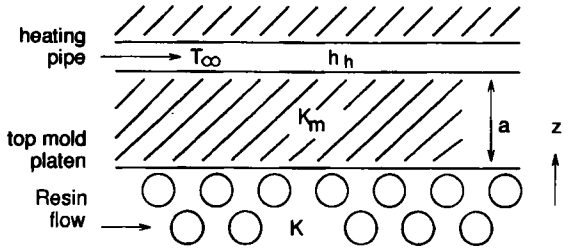

Figure 3. Configuration used to obtain the temperature boundary condition at the mould platens

approximation is a constant temperature at the mould platens.[20] However, experimental studies have shown that the mould temperature will undergo significant fluctuations during the mould filling.[18] A more general boundary condition may be derived by a quasi-steady-state analysis of a typical mould configuration. A mould is assumed to have a heating pipe at a distance a from the mould wall as shown in Figure 3. The pipe is heated with a fluid at temperature T_∞ and there is a heat transfer coefficient h_h between the heating fluid and the pipe. The heat transfer coefficient between the resin and the mould wall is h_m. This configuration results in the boundary condition

$$\frac{\partial \theta}{\partial z} + C_{bc}\theta = 0, \tag{7}$$

where $\theta = T - T_\infty$ and

$$C_{bc} = \frac{1}{\kappa} \frac{1}{1/h_h + 1/h_m + a/\kappa_m}. \tag{8}$$

Here κ_m is the conductivity of the mould material. This formulation results in one boundary constant C_{bc} which is zero for the insulated or adiabatic case boundary condition and which is infinity when one wants to specify a constant temperature boundary condition. The heat transfer coefficient between the mould platen and the resin needs to be measured experimentally, since there is no theoretical way to predict this parameter.

For a realistic value for C_{bc}, consider that the heat transfer coefficient between steam and metal is around 7000 W m^{-2} K^{-1} and the conductivity of steel is around 500 W m^{-1} K^{-1}. For a steam-heating element located 10 cm behind the mould surface the resulting boundary condition constant would be of the order of 50 m^{-1}.

Owing to the transient nature of the problem, one has to take into account the internal energy of the fibre preforms which are impregnated by the moving flow front. This is done by performing local heat balance at the flow front, which takes into account the convection into the unsaturated medium.

The last boundary condition is the specification of the fluid temperature at the injection gates. This condition should only be applied during the mould-filling stage. Once the mould is full, the fluid injection stops and this boundary condition vanishes. The energy equation reduces to a balance between conduction across the thickness and heat generation, since there is no longer any convection.

2.1.2. Resin cure. The only term which still needs to be defined in the energy equation is the source term. To describe the heat generation due to cure in the energy equation (5), a model

that is well suited to represent the curing behaviour of polyester as well as epoxy resin is used.[23–25] It assumes the specific energy generated during curing is proportional to the rate of the reaction:

$$\dot{s} = R_\alpha E_\alpha, \tag{9}$$

where R_α is the rate of the reaction and E_α is the reaction energy. The reaction rate itself is a function of temperature and the extent of the reaction:

$$R_\alpha = (k_1 + k_2 \alpha^m)(1 - \alpha)^n. \tag{10}$$

The values of k_1 and k_2 are Arrhenius functions of temperature:

$$k_1 = A_1 \exp\left(\frac{E_1}{RT}\right), \tag{11a}$$

$$k_2 = A_2 \exp\left(\frac{E_2}{RT}\right), \tag{11b}$$

where R is the universal gas constant. The constants A_1, A_2, E_1, E_2, m and n are material constants which may be determined by differential scanning calorimetry for a particular resin system.[18]

It should be noted, however, that many semi-empirical models for resin cure exist. Most describe the behaviour of certain resins well but fail to accurately describe the behaviour of other resins. Therefore it is essential to determine which model properly describes the resin one intends to use if an accurate cure solution is desired.

Since the resin flows through the mould, an expression for the convection of the degree of cure is necessary. Conservation of species may be expressed by a continuity equation

$$\frac{\partial \alpha}{\partial t} + \bar{u}_x \frac{\partial \alpha}{\partial x} + \bar{u}_y \frac{\partial \alpha}{\partial y} = R_\alpha. \tag{12}$$

2.1.3. Temperature-, cure- and strain-rate-dependent viscosity. Finally, for non-isothermal and shear-thinning flow behaviour, one needs to consider that the resin viscosity is not a constant but a function of temperature, strain rate and cure. The strain rate behaviour for a power-law fluid and a Carreau fluid is described in detail in our previous papers.[1,9] The temperature-dependent behaviour is traditionally modelled using an Arrhenius equation which describes the viscosity as an exponential function of temperature:

$$\eta = \eta_0 \exp(-a\theta), \tag{13}$$

where $\theta = T - T_0$ with T_0 being some reference temperature at which the viscosity is equal to η_0.

In addition, the viscosity of the resin will change as the cure proceeds. Models that represent the dependence of viscosity on the degree of cure and temperature are referred to as chemorheological models. A model that describes the behaviour of polyester resins well is described in Reference 26.

The variation in the viscosity with temperature and degree of cure introduces a two-way coupling between the fluid flow and energy equations. Since the degree of cure is close to zero until the mould is filled, it does not cause any numerical problems. Also, a three-dimensional temperature solution is coupled with a two-dimensional pressure solution through the viscosity.

This is accomplished by calculating the average viscosity through the thickness $\bar{\eta}$ by integrating across the thickness h at each point in the plane of the mould:

$$\frac{1}{\bar{\eta}} = \frac{1}{h}\int_0^h \frac{1}{\eta}\,\mathrm{d}l. \tag{14}$$

This value may then be used in calculating the pressure distribution in Equation (3).

3. NUMERICAL IMPLEMENTATION

In the previous section the theory governing the flow through fibrous media was discussed. In this section we present the approach to develop a numerical simulation that can describe the macroscopic flow front of non-isothermal flow through an arbitrary thin shell three-dimensional geometry.

An important issue in the simulation of mould-filling processes such as RTM, compression moulding and injection moulding is the numerical treatment of the transient free surface or the moving boundary (the boundary where the fluid is displacing air in the mould cavity). The material inside the mould is constantly changing shape as it flows. This makes it necessary to redefine the geometry of the domain in which the governing equations are to be solved after each successive time step. The governing equations for these filling models have been solved by a variety of numerical techniques.[12,13,27–32] The techniques which require redefining of the mesh and mesh generation for mould-filling problems have the drawback of being tedious, and bookkeeping when two flow fronts merge or for flow around inserts can be quite cumbersome. Mesh generation even after a few time steps could be the most tedious part of the simulation. Finite element/control volume (FE/CV) is an attractive alternative, since one does not need to remesh it and it is possible to simulate filling in thin cavities with highly complex geometries. A key feature of the FE/CV method is a rough approximation of the domain shape combined with a rigorous accounting of the mass conservation. The traditional control volume approach introduces an error when skewed elements are used. For these types of meshes the mass conservation condition may be violated.[33]

3.1. Finite element/control volume method

One needs to discretize the governing equation (3) in a flow domain changing with time in order to capture the physics of flow through an arbitrary three-dimensional thin shell geometry. The discretized governing equation can then be solved, and once the pressures are known, the change in the shape of the fluid domain needs to be calculated. This is accomplished by a numerical simulation based on the finite element/control volume method. The part geometry is modelled as a thin shell in three-dimensional space using triangular and/or quadrilateral elements of specified thickness. Different elements may have a different thicknesses to account for variations in the gap height of the mould. Galerkin finite element equations are used to solve for the pressure at any instant during the filling process and the control volume approach is used to advance the free surface flow front.

3.1.1. Pressure solution. Bilinear basis functions are used in the present discretization of the governing equation (3). This results in C_0 continuity of the resulting pressure solution. The pressure values will be continuous across elements, but the first derivatives may not be. Galerkin's method, in which the interpolation functions are the weighting functions, is used. The element

stiffness components are assembled on a nodal basis, resulting in a set of algebraic equations in terms of the stiffness matrix $[[S^e]]$ and the nodal pressure vector $[P]$ for the whole fluid domain:

$$[[S^e]][P] = [0]. \tag{15}$$

The element stiffness matrix components are calculated using a Gaussian quadrature integration technique. After the stiffness matrix is assembled for all elements in the fluid domain, it is modified to account for the zero pressures at the free surface flow front and for the specified pressures at the fluid injection locations.

Injection at constant flow rate is incorporated by modifying the forcing vector (right-hand-side vector) at the injection nodes. Since the left-hand side of the equation represents the continuity condition, the value of the forcing vector specifies the amount of mass generated per unit time at the selected node. If an injection flow rate Q_{bc} is specified at a given node i as a boundary condition, then the forcing vector for row i in equation (15) will be modified according to

$$[[S^e]]P_i = Q_{bc}. \tag{16}$$

Sources which are not specified at a node but in the interior of the element are not considered in the current simulation.

The stiffness matrix is assembled on an element basis using a local element co-ordinate system. The permeability tensor needs to be transformed from the global (1, 2) co-ordinate system to the local element (x, y) co-ordinate system using a regular matrix rotation transform:

$$\begin{pmatrix} K_{xx} & K_{xy} \\ K_{yx} & K_{yy} \end{pmatrix} = \begin{pmatrix} \cos\theta & \sin\theta \\ -\sin\theta & \cos\theta \end{pmatrix} \begin{pmatrix} K_{11} & K_{12} \\ K_{12} & K_{22} \end{pmatrix} \begin{pmatrix} \cos\theta & -\sin\theta \\ \sin\theta & \cos\theta \end{pmatrix}, \tag{17}$$

where θ is the angle between the two co-ordinate systems.

In complex three-dimensional geometries it is often not possible to use the global co-ordinate system, with respect to which the mould geometry is specified, as a reference for the permeability tensor. The projection of any of the three global co-ordinate axes on the mould surface is used as the 1-axis with respect to which the material properties in that section of the mould are specified. The simulation then performs the rotation from that co-ordinate system to the local element co-ordinate system to assemble the stiffness matrix. Figure 4 shows an example of a

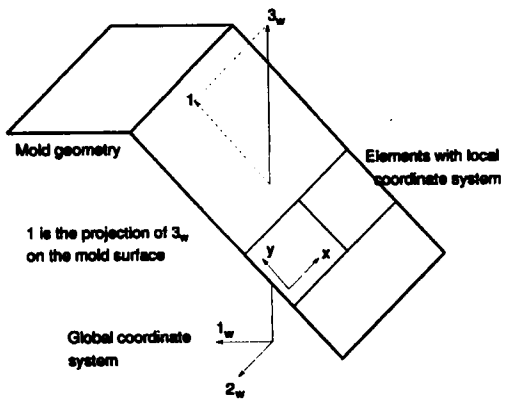

Figure 4. Example of a mould geometry with the various co-ordinate systems used in specifying the permeabilities

mould surface with the different co-ordinate systems. Here the 3_w-axis of the global co-ordinate system is chosen as the reference axis, which yields the 1-axis when projected on the mould surface. The angle of rotation between the 1-axis and the local element x-axis is in this case $-90°$. After the stiffness matrix is assembled and all boundary conditions are applied, the system is solved for the unknown pressures using a standard matrix inversion technique.

For generalized Newtonian fluids, where the viscosity is a function of the strain rate of the fluid, an iterative solution procedure is required. The viscosities obtained at the previous time step are used as a first guess for the local viscosities at the present time step. With these values the stiffness matrix is assembled and the pressures are calculated. The viscosities are then recalculated throughout the mould and the governing pressure equation is solved. This iterative procedure is continued until the maximum relative difference between nodal pressure values at subsequent iterations is less than a user-specified convergence criterion. To increase the rate of convergence, an underrelaxation technique is used. In applying this technique, the pressure used to calculate the new viscosity for the next iteration is selected according to the equation

$$P_i = \lambda P_i^k + (1 - \lambda) P_i^{k-1}, \tag{18}$$

where λ is the underrelaxation parameter, P_i^k are the nodal pressures just calculated and P_i^{k-1} are the pressures obtained during the previous iteration. From experience it is found that for power-law fluids the power-law exponent is in general a good choice for the underrelaxation parameter.

Once the nodal pressures are known, the velocity field is obtained from Darcy's law by using the derivatives of the interpolation functions to obtain the pressure gradient. The derivatives of the interpolation functions are evaluated at the element centroids for the greatest accuracy, resulting in elemental rather than nodal velocities. It is not necessary to solve for the velocity if one employs the control volume approach to calculate the location of the free surface of the fluid.

3.1.2. Control volume approach. After solving for the pressures, the position of the free surface flow front needs to be updated. The movement of the transient free surface flow front is calculated using the control volume approach. This approach is pragmatic and very efficient. It allows one to monitor the degree to which each element is filled with fluid. First the traditional control volume approach will be discussed. Since the traditional control volume approach results in a mesh-dependent error in the location of the free surface flow front, a modified control volume approach is suggested which eliminates this type of error.

3.1.3. Traditional control volume approach. The mould geometry is not only divided into elements but also into control volumes, by associating one with every node. The traditional control volume is bound by the element centroids and the element mid-sides. A typical configuration is shown in Figure 5. The flow rate between control volumes is calculated by multiplying the superficial velocities by the area connecting two control volumes. The control volumes associated with nodes i and j are indicated by the shaded area in Figure 5. Assuming a linear pressure profile between the nodes and using the average element height, the equation for the flow rate q_{ij}, from node i to node j may be written as

$$q_{ij} = -\frac{W}{\eta_{\text{eff}}} \frac{h_i + h_j}{2} \left(K_{xx} \frac{P_i - P_j}{l} + K_{xy} \frac{\partial P}{\partial n} \right), \tag{19}$$

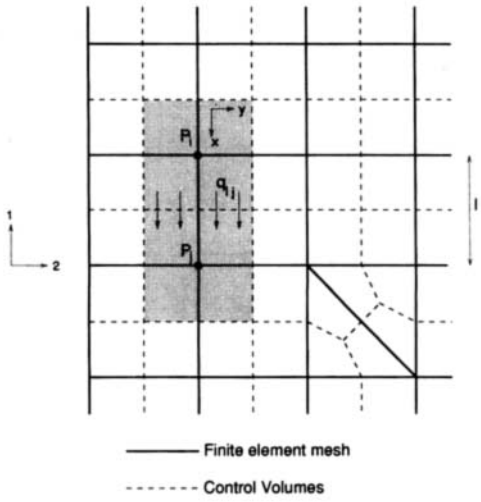

Figure 5. Finite element mesh with control volumes

where W is the width of the connecting area and l is the distance between nodes i and j. The permeabilities K_{ij} are taken in the local element co-ordinate system (x, y) as opposed to the global mould co-ordinate system $(1, 2)$. $\partial P/\partial n$ is the pressure gradient perpendicular to the direction of flow and is obtained by taking the average of the pressure gradient normal to the direction of flow in the two adjacent elements. Since the pressures are already known at this stage, the value of the viscosity η_{eff} is also known at each nodal point, so the generalized Newtonian case presents no special problem.

Once the flow rates between control volumes are known, the total net flow into each control volume j may be calculated as

$$Q_j = \sum_{i=1}^{N} q_{ij} \Delta t, \tag{20}$$

where N is the number of control volumes connected to control volume j and Δt is the size of the time step.

Nodal fill factors are used to track the moving flow front. The fill factor for each node is the fraction of its control volume occupied by the fluid. As shown in Figure 6, the fill factor is zero for an empty control volume and unity for a completely filled one. The nodal fill factors are used in determining where to apply the flow front boundary conditions for the pressure solution. Pressures are calculated at completely filled nodes, while empty nodes are ignored. Partially filled nodes are assumed to lie close to the front and the flow front boundary condition is applied there. The size of the time step is calculated such that only one control volume fills at each time step, thus modifying the boundary condition at only one node. The flow front is advanced at each time step by updating the fill factors, using the total flow rate into a control volume from equation (20). With this technique one can fill thin cavities with highly complex geometries in three-dimensional space and also account for the variation in the gap height of the part.

This implementation of the control volume approach introduces errors in the flow rates which depend on the mesh geometry. This error can be demonstrated by using the simple mesh configuration in Figure 7. The mesh consists of triangular elements, with one side of the triangle

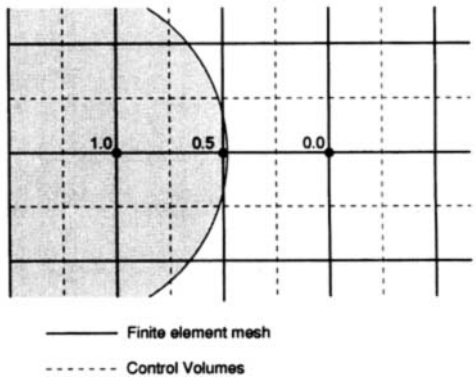

Figure 6. Nodal fill factors. The shaded region represents the filled area of the mould

having a length a and the other side a length b. In this one-dimensional example the pressure drop will be linear and the pressure difference between the two lower rows of nodes is $\Delta P = P_2 - P_1$. The total flow into the shaded control volumes using equation (19) is

$$Q_{\text{in}} = \Delta P\left(\frac{a}{b} + \frac{2}{a/b + b/a}\right), \tag{21}$$

assuming the permeability, viscosity and element thickness to be equal to unity. Theoretically, the total flow rate should be the pressure gradient times the connecting area, given by

$$Q_{\text{in}}^{\text{th}} = 2a\,\frac{\Delta P}{b}. \tag{22}$$

It is easily seen that when the triangles are equilateral ($a = b$), the theoretical or exact flow rate corresponds to the actual flow rate. However, as the elements become more skewed, the

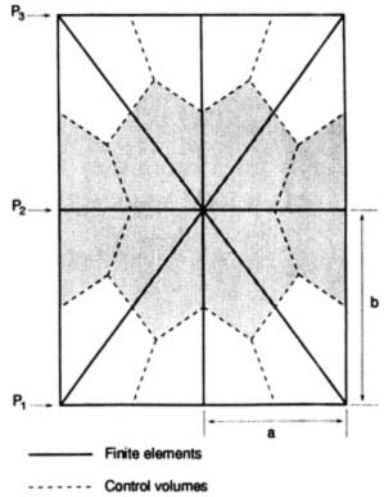

Figure 7. Triangular mesh to demonstrate the error in the traditional control volume approach

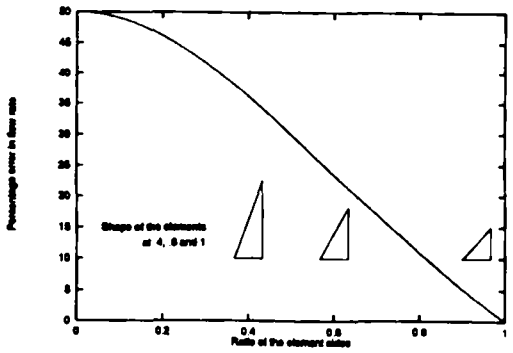

Figure 8. Error percentage resulting from the control volume method versus the ratio of the element sides

difference increases rapidly. Figure 8 shows the error percentage versus the ratio of the element sides. If the ratio a/b equals 0·6, the flow rate from the control volume method is 25% greater than theoretically calculated value. Note that this error is dependent only on the ratio of the element sides. Mesh refinement, while keeping the element shape the same, will not increase the accuracy of the control volume method.

3.1.4. Element control volume method. Both the intrinsic errors which occur in the traditional control volume method can be corrected by modifying the geometric location of the control volumes. We propose to use an element control volume method. In this method the elements and the control volumes coincide. This technique has a number of distinct advantages over the traditional control volume method. First, it eliminates the error caused when the elements are not exact rectangles or equilateral triangles. Second, it eliminates any violation of the continuity condition in a control volume. The finite element equations are solved on an element basis and therefore the pressure distribution in each element obeys the continuity condition. The resulting flow rates will then also be in accordance with the continuity condition. There may still be some mass discontinuity between elements, but this will not effect the shape of the flow front or the heat transfer calculations.

The application of the finite element boundary conditions is slightly different than in the traditional control volume approach. The node at which the boundary condition is applied should be as close to the actual flow front as possible. Since the nodes are no longer at the centre of the control volumes but make up the corners of a control volume, the boundary conditions are applied based on the fill factor of the element under consideration and the fill factor of the neighbouring elements. If an element is less than half full, the boundary conditions are applied at the nodes of the element which also connect to a full element, such as node 2 depicted in Figure 9. If an element is more than half full, the conditions are applied at the nodes of the element which also connect to an empty element, such as nodes 1, 3 and 4 shown in the same figure. All other nodes connected to completely empty elements are ignored and the pressure is calculated at the remaining nodes.

In this approach the boundary conditions are modified when a fill factor increases from less than half to more than half. Therefore the size of the time step is restricted by the first control volume that fills halfway. In the traditional control volume method the time step was based on an empty or partially full control volume being filled completely. A control volume filling completely does not change the boundary conditions in the element control volume method.

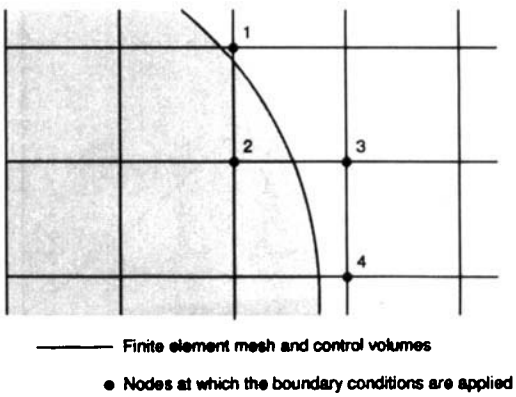

Figure 9. Nodes at which the flow front pressure boundary condition is applied using the element control volume method

Therefore, in one time step a control volume that is more than half full may fill completely and the neighbouring control volume may fill halfway. Thus the flow front may be advanced by a full element in a given time step. If an element is less than half full, the pressure will be zero at all nodes of the element, resulting in a zero pressure gradient inside the element. To fill this element, the flow rates calculated from the neighbouring elements are used.

Once the pressure distribution is known after solving the finite element equations, the flow rates between the control volumes are calculated using

$$q_{ij} = -\frac{W}{\eta_{\text{eff}}}\frac{h_i + h_j}{2}\left(K_{xx}\frac{\partial P}{\partial x} + K_{xy}\frac{\partial P}{\partial y}\right), \tag{23}$$

where the pressure gradients are calculated from the pressure solution using the shape functions N_i of the element:

$$\frac{\partial P}{\partial x} = \sum_{i=1}^{n}\frac{\partial N_i}{\partial x}P_i. \tag{24}$$

In these equations, similarly to the traditional control volume approach, (x, y) is the local co-ordinate system with x aligned in the direction of flow, as opposed to the global mould co-ordinate system.

It is clear that the element control volume method does add some complexity in applying the boundary conditions and advancing the flow front in comparison with the traditional control volume method. However, the extra computational effort required for the element control volume method is less than 5% in terms of the total simulation CPU time.

Virlouvet and Tucker[33] recently proposed a method similar to the element control volume approach. Their method is based on retaining the stiffness matrix and multiplying it by the obtained pressures to find the total flow rates into each control volume. Although their method results in the same total flow into each control volume as our element control volume method, no specific information is available about the flow rates between two connecting elements. When solving for isothermal flow, this is no consequence, but for non-isothermal mould filling one needs this information to take into account convection between control volumes.

The main characteristic of the element control volume method is that it eliminates the mesh-dependent error produced by the traditional control volume method. Second, it eliminates

the discretization error due to the C_0 continuity of the pressure solution inside the control volume. Instead, there will be a discretization error in between two control volumes (i.e. the flow rate out of one element may not exactly equal the flow rate into the neighbouring element). However, this error does not influence the temperature solution, unlike the error in the traditional control volume method. The element control volume method increased accuracy by far outweighs the slight increase in CPU time.

3.2. Temperature solution

The temperature and degree of cure profiles are obtained using a partially implicit finite difference method. Owing to the heat transfer from the top and bottom mould platens to the resin and preform, one must account for the conduction in the thickness direction. Consequently, the temperature distribution is calculated in three dimensions. The convective terms in the energy equation and the convection of degree of cure are taken into account using a control volume method, consistent with the approach used to solve for the movement of the free surface flow front.

A modified Crank–Nicolson approach is used to discretize the energy equation (5). This method has the advantage that it is unconditionally stable and has little upwinding effects.[34,35] Since the control volumes are defined to coincide with the elements in the element control volume approach, the control volumes for the energy calculations are defined accordingly. Each control volume defined for the flow analysis is subdivided through the thickness into control volumes for the temperature analysis as shown in Figure 10. The energy balance is carried out in each control volume. This implies that the temperature will be obtained at the centroid of each control volume. One can then calculate nodal temperatures through the thickness by taking the average of the temperatures of the connecting control volumes.

The energy balance for a typical control volume i with the centre at through-thickness location z and height Δz as depicted in Figure 11 is

$$V^{n+1}(T^{n+1} - T^n) + \Delta V c_1 T^n + \Delta V(1 - c_1)(T^n - T_g) = \sum_{j=1}^{N} q_{ji}\Delta t c_1 T_{j,i} + c_2 \Delta t A\left(\left.\frac{\partial T}{\partial z}\right|_{z+\Delta z/2} - \left.\frac{\partial T}{\partial z}\right|_{z-\Delta z/2}\right) + \dot{S} c_3 \Delta t, \tag{25}$$

where the superscript n denotes the known values at the current time step and $n + 1$ the values to be calculated at the next time step. T_g is the initial temperature of the fibre preform and A is the surface area of the top and bottom of the control volume through which the conduction

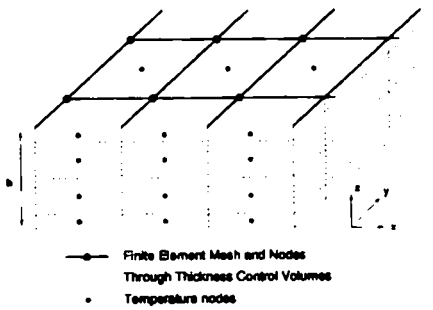

Figure 10. Control volumes used in the temperature and cure analysis

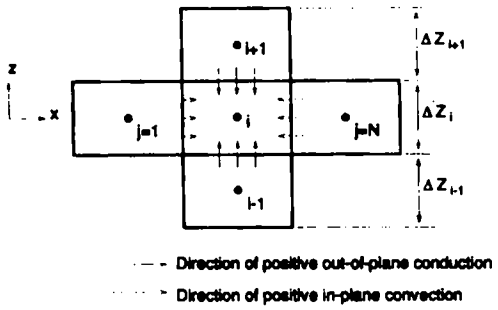

Figure 11. Cross-section of a typical control volume and the neighbouring control volumes used in the temperature solution

takes place. The convection contribution is taken into account by the summation over all N neighbouring control volumes, where q_{ji} is the flow rate from the neighbouring control volume into the one under consideration and $T_{j,i}$ is the temperature at the interface between two control volumes. $\dot{S}$ is the total rate of heat generation in the control volume. The terms ΔV arise from the flow front boundary condition. ΔV is the fraction of the control volume which is filled during the current time step and V^{n+1} is the total fraction of the control volume which is occupied by fluid. If the control volume is completely filled, the ΔV terms will vanish and V^n and V^{n+1} will equal the total volume of the control volume. The constants c_k are related to the thermal properties of the fibre and resin as

$$c_1 = \frac{\phi \rho_r c_{p_r}}{\phi \rho_r c_{p_r} + (1-\phi)\rho_f c_{p_f}}, \tag{26a}$$

$$c_2 = \frac{K}{\phi \rho_r c_{p_r} + (1-\phi)\rho_f c_{p_f}}, \tag{26b}$$

$$c_3 = \frac{\phi}{\phi \rho_r c_{p_r} + (1-\phi)\rho_f c_{p_f}}. \tag{26c}$$

In using the Crank–Nicolson method, one essentially expands the solution about the time $t + \Delta t/2$. This results in the following expressions for the expansion of the variables used in equation (25):

$$T_{j,i} = \frac{1}{2}\left(\frac{T_i^n + T_i^n}{2} + \frac{T_i^{n+1} + T_j^{n+1}}{2}\right), \tag{27a}$$

$$\left.\frac{\partial T}{\partial z}\right|_{z+\Delta z/2} = \frac{T_{i+1}^n - T_i^n}{\Delta z_i - \Delta z_{i+1}} + \frac{T_{i+1}^{n+1} - T_i^{n+1}}{\Delta z_i - \Delta z_{i+1}}, \tag{27b}$$

$$\left.\frac{\partial T}{\partial z}\right|_{z-\Delta z/2} = \frac{T_i^n - T_{i-1}^n}{\Delta z_i - \Delta z_{i-1}} + \frac{T_i^{n+1} - T_{i-1}^{n+1}}{\Delta z_i - \Delta z_{i-1}}, \tag{27c}$$

$$\dot{S} = \tfrac{1}{2}(\dot{s}^n \rho_r V^n + \dot{s}^{n+1} \rho_r V^{n+1}). \tag{27d}$$

As shown in Figure 11, $i + 1$ denotes the control volume above the one under consideration and $i - 1$ is the one below. To account for the boundary conditions at the top and bottom mould

walls, the following expressions are used for the nodes at the mould wall:

$$\left.\frac{\partial T}{\partial z}\right|_{\text{top}} = \tfrac{1}{2}[C'_{\text{bc}}(T_\infty - T_i^n) + C'_{\text{bc}}(T_\infty - T_i^{n+1})], \tag{28a}$$

$$\left.\frac{\partial T}{\partial z}\right|_{\text{bottom}} = \tfrac{1}{2}[C'_{\text{bc}}(T_i^n - T_\infty) + C'_{\text{bc}}(T_i^{n+1} - T_\infty)]. \tag{28b}$$

Since the temperature node is at the centroid of the control volume and not at the mould wall, the mould wall temperature is

$$T_{\text{wall}} = T_i \pm \frac{\partial T}{\partial z}\frac{\Delta z}{2}. \tag{29}$$

Substituting this back in equation (7) results in the following expression for C'_{bc}:

$$C'_{\text{bc}} = \frac{1}{1/C_{\text{bc}} + \Delta z_1/2}. \tag{30}$$

This boundary condition is implicit in nature, since it contains the temperature at the next time step.

In order to solve this set of equations, an iterative procedure is used. Since the node numbering of the finite element mesh specified by the user of the simulation is arbitrary, assembling the temperature equations for all control volumes would result in a sparse matrix. However, the through-thickness control volumes are numbered consecutively by the simulation, e.g. $i-1$, i and $i+1$ as shown in Figure 11. The neighbouring j-nodes may be numbered arbitrarily. In order to avoid excessive computer time and memory requirements, the temperature field is solved successively at each in-plane location through the thickness. Assembling the energy balance equations (25) for a row of through-thickness nodes results in a banded tridiagonal system that can be solved efficiently using the Thomas algorithm:[35]

$$[[S_{\text{T}}]]\begin{bmatrix}\vdots\\ T_{i+1}\\ T_i\\ T_{i-1}\\ \vdots\end{bmatrix} = [R], \tag{31}$$

where $[[S_{\text{T}}]]$ is a triadiagonal matrix. The terms from the energy balance that depend on the in-plane neighbouring temperatures T_j are contained in the right-hand-side vector R. This solution procedure is applied to all in-plane mould locations and repeated until a convergence criterion is satisfied:

$$\varepsilon \geqslant \frac{T_i^k - T_i^{k-1}}{T_i^k} \quad \forall i, \tag{32}$$

where ε is the magnitude of the convergence criterion and k is the iteration number. A Gauss–Seidel iteration is used so that the right-hand-side vector reflects the most recently obtained temperature values.

3.2.1. Cure solution. Since the source terms as given by equation (10) to obtain the temperature solution is non-linear, the value of the temperature at the most recent iteration is used to obtain

s^{n+1} in equation (27). Once numerical convergence is achieved and the temperatures are known, one can calculate the final rate of the reaction from equation (10). To account for the convection of the extent of the reaction, α, the following equation is used for conservation of species:

$$V^{n+1}\alpha_i^{n+1} = (V^{n+1} - \Delta V)\alpha_i^n + \sum_{j=1}^{N} q_{ji}\alpha_j^n + \frac{d\alpha}{dt}\Delta t. \tag{33}$$

This equation represents a conservation of species or the extent of the reaction. In using this equation, α is linearized owing to the convective terms. Since the values of the extent of the reaction in neighbouring elements are close, this assumption is justified.

3.2.2. Average effective viscosity. The temperature and cure kinetics are coupled with the fluid flow equations by the viscosity. Once the temperature and the extent of cure are known in each control volume, the viscosity may be calculated using equation (13) if the cure reaction has not initiated, or with a chemorheological model after the curing initiates.[26] To obtain the viscosity in the plane of each finite element used in the pressure solution, the average effective through-thickness viscosity is calculated using

$$\bar{\eta}_{\text{eff}} = \frac{1}{h}\sum_{i=1}^{N} \eta_i \Delta z_i, \tag{34}$$

where η_i is the viscosity at each through-thickness node and N is the number of nodes through the thickness. The value of η_{eff} is used to calculate the pressures and advance the flow front at the next time step.

3.3. Summary of numerical implementation

Figure 12 shows an overview of the numerical simulation, titled LIMS, an acronym for Liquid Injection Moulding Simulation. The user of the simulation supplies the mesh, permeabilities, gate locations and flow rates or injection pressures, material constants (rheological, thermal and chemical), the number of nodes through the thickness for the temperature simulation, and the temperature boundary condition constants. With this information the pressure distribution in the mould may be calculated. In the case of shear-thinning fluids the viscosity based on the pressure solution is calculated and then the pressure distribution is recalculated. This procedure is repeated until the pressure solution converges to within the user's specification. Now the flow rates between the control volumes may be calculated and a time step chosen such that only one control volume fills up to 50%, ensuring that the boundary conditions change only at one location. Once the time step is known, the fill factors may be updated based on the calculated flow rates. Then the temperature distribution is calculated as discussed in the previous subsections. Simultaneously, the extent of the reaction is updated in each control volume and the average through-thickness viscosity is calculated. A test is performed to check whether all the fill factors equal unity, which signifies that the mould is full. If this is not the case, the simulation solves for the pressure again and repeats the cycle until the mould has filled. Once the mould is full, only the temperature and cure kinetics equations of the numerical implementation need to be solved, until the extent of the reaction equals unity in all control volumes and the part has cured completely.

Note that the heat transfer and the flow parts of the simulation are coupled. The flow depends on the heat transfer through the viscosity, while the heat transfer depends on the flow through

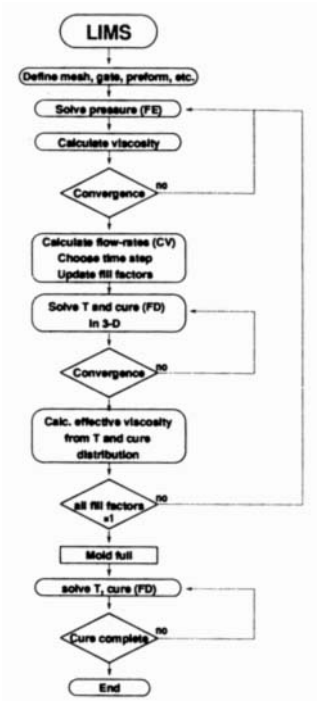

Figure 12. Flowchart of the numerical simulation

the convection of the fluid. The simulation does allow one to solve for the flow and heat transfer in an iterative manner. However, in our experience this is not necessary and does not significantly enhance the accuracy of the solution. Table I provides an overview of the input parameters necessary to perform the various simulation steps and the output available from the simulation.

3.4. Verification of the numerical simulation

The simulation was verified by comparing the results with analytical solutions, checking convergence with mesh refinement and by comparison with experiments.[36] In this subsection we will compare the results of our simulations with known closed form solutions for four test problems. The details are documented in Reference 36. The first is a one-dimensional flow into a mould with varying gap width. The second case is flow of a power-law fluid into a rectangular mould. Since the equations for this case are non-linear, the iterative procedure is used to obtain the numerical solution. Third, an injection of a fluid in the centre of a square mould with an anisotropic fibre medium is studied. The fourth test case verifies the non-isothermal filling of a mould.

3.4.1. Mould with varying gap width. The mould under consideration for this test case is shown in Figure 13. Fluid is injected from one end into a mould which has a different gap width in the first section of the mould than in the second section of the mould. Using Darcy's law and applying the continuity condition at the cross-section where the change in gap width occurs yields the following equation for the total fill time of the mould:

$$t_{\text{fill}} = \frac{\eta}{KP_i}\left(\tfrac{1}{2}(L_1^2 + L_2^2) + \frac{h_1}{h_2} L_1 L_2\right), \tag{35}$$

Table I. User-specified input and output from the simulation steps

	Solve pressure
Input	In-plane mesh node co-ordinates x, y, z Element connectivity and thickness h Injection location and pressure or flow rate Chemorheological parameters Preform permeabilities K_{11}, K_{22}, K_{12} for each material Fluid rheological properties η (Newtonian) or m, n and/or $\tau_{1/2}$ (shear-thinning)
Output	Nodal pressures Nodal velocities
	Calculate viscosity
Output	Nodal viscosities
	Test for convergence
Input	Convergence criterion Relaxation parameter (optional)
	Calculate flow rates
Output	Current time in simulation Flow front position
	Solve temperature
Input	Number of through-thickness nodes Through-thickness node distribution Mould boundary condition constant C_{bc} and temperature T_∞ Resin thermal properties $\rho_r c_{p_r}$ and κ_r Fibre thermal properties $\rho_f c_{p_f}$ and κ_f Porosity ϕ Viscosity temperature dependence parameters
Output	3D temperature field
	Solve cure
Input	Resin cure model parameters, equation (10) Chemorheological parameters
Output	3D cure distribution

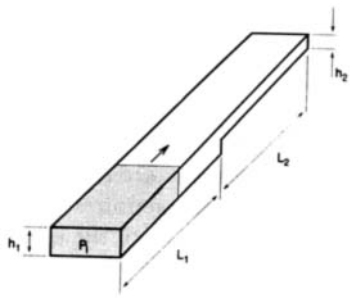

Figure 13. Mould with varying gap width

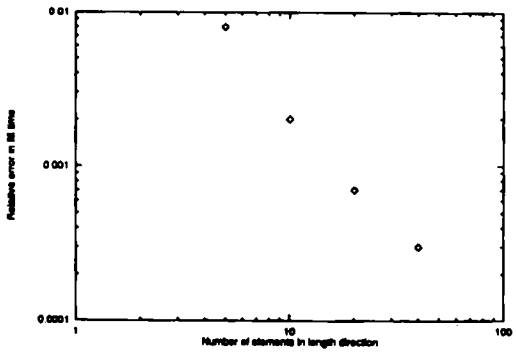

Figure 14. Comparison between the theoretical and numerically obtained power-law fluid for a number of different mesh sizes

where P_i is the injection pressure and L_i and h_i are the length and gap width respectively of the two sections of the mould. Figure 14 compares the fill time from the numerical simulation with the theoretical fill time for a number of different mesh sizes. K, η and P_i were all set to unity, $L_1 = 0{\cdot}4$, $L_2 = 0{\cdot}6$, $h_1 = 1$ and $h_2 = 0{\cdot}3$ for this test case. The theoretical mould fill time is $t_{\text{fill}} = 1{\cdot}32$. The number of elements in the length of the mould was varied and two elements were used in the mould width.

Even a very coarse mesh gives excellent results for this mould configuration and there is no significant improvement in the numerical results with mesh refinement. Since in this case the pressure drop in both sections of the mould is linear, the simulation can capture the pressure profile exactly at each time step. Also, since all elements are the same size, this pressure profile will be exactly the average profile during the filling of the control volumes. Thus even a coarse mesh can capture the physics of this process very well and yield accurate numerical results.

3.4.2. Power-law fluid. To verify the accuracy of the iterative procedure used to calculate the mould filling using power-law fluids, a simple rectangular mould is used. The fluid is injected from one side into the mould, resulting in a one-dimensional flow as the mould fills. In this case the capillary model was used to obtain an expression for the effective viscosity.[1] The fill time of the mould can be calculated analytically as

$$t_{\text{fill}} = \frac{\alpha + 3}{4(\alpha + 1)} \frac{1}{KC_\tau^{\alpha - 1}} \left(\frac{m}{P_i}\right)^\alpha L^{\alpha + 1}, \tag{36}$$

where L is the mould length and C_τ is the constant of proportionality between the wall shear stress and the pressure gradient. Figure 15 compares the numerically obtained and theoretical fill times for m, K and P_i all unity. With a power-law index of 0·5, resulting in $\alpha = 2$ and a mould length of 20, the theoretical time required to fill the mould is 93·3. Using the power-law index as the underrelaxation parameter requires an average five iterations per time step to achieve convergence to within 10^{-5}. From the figure it is clear that the numerical solution tends to the analytical answer as the mesh is refined; however, using more than 50 elements in the length direction does not increase the accuracy significantly and the rate of numerical convergence decreases.

3.4.3. Injection in the Centre of a Square Mould. The last comparison for the isothermal case between numerical and analytical data was done using a square flat mould with an injection

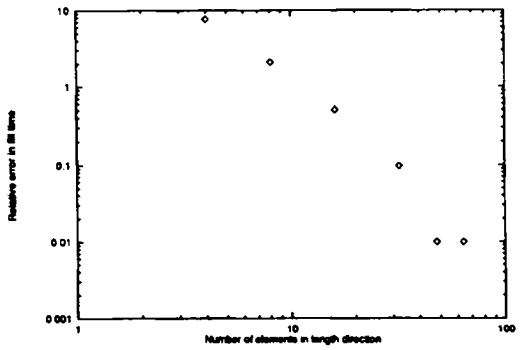

Figure 15. Relative error in the fill time for one-dimensional flow of a power-law fluid for a number of different mesh sizes

gate at the centre. The permeabilities were 1 and 0·1 respectively in the x- and y-directions representing a unidirectional fibre mat. As shown in Reference 5, the flow front should progress as an ellipse with the ratio of the major and minor axes equal to the square root of the ratio of the principal permeabilities. In this case the mould was filled at a constant flow rate. Since the area of an ellipse with major and minor axes a and b respectively is πab, mass continuity predicts the shape of the flow front to be

$$l = \frac{Q_i t}{\pi \sqrt{(K_{11} K_{22})}}, \tag{37}$$

where $l\sqrt{K_{11}}$ is the position of the flow front along the x-axis and $l\sqrt{K_{22}}$ is the position along the y-axis. Q_i is the injection flow rate. Figure 16 plots the combined error in the location of the flow front along the x- and y-axes for three different mesh sizes, 10 × 10, 25 × 25 and 50 × 50.

Note that the error increases at the start of the simulation and then levels off. The pressure distribution in the mould behaves like $\log(1/r^2)$, where r is the distance from the injection gate. At the onset of the simulation the pressure gradient will vary greatly over a short distance. The simulation has to approximate this behaviour by assuming a constant gradient in each element,

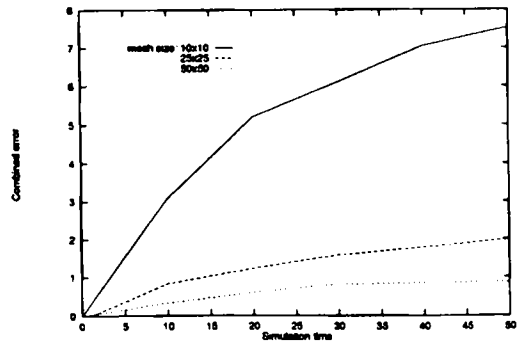

Figure 16. Percentage error in the location of the flow front for three mesh sizes for injection into the centre of a square mould

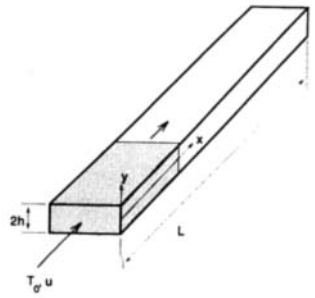

Figure 17. Mould and co-ordinate frame used in the theoretical verification of the temperature distribution

and makes a certain error in doing so. As the mould fills, the pressure gradient will become smoother, and the simulation produces more accurate results.

3.4.4. Non-isothermal filling with constant temperature boundary condition. In this case the boundary condition constant, C_{bc} was set to $5000\,m^{-1}$, indicating a constant temperature boundary condition. The temperature of the mould platens was set to 100°C and the fluid injected at 0°C and at a constant flow rate. The effect of the preform was ignored in this case and therefore the porosity was set to unity. Figure 17 shows the mould and the co-ordinate frame used in this simulation.

Ignoring conduction in the in-plane direction, an analytical solution for the temperature profile is

$$\theta(x', y) = \sum_{n=0}^{\infty} \theta_0 \frac{2(-1)^n}{\lambda_n h} \exp(-\lambda_n^2 x') \cos(\lambda_n y), \tag{38}$$

where

$$x' = \beta x/u, \tag{39}$$

$$\theta = T - T_{\text{mould wall}}, \tag{40}$$

$$\lambda_n = (2n + 1)\pi/2h. \tag{41}$$

Here β is the diffusivity of the fluid, defined as $\kappa/\rho_f c_{p_f}$, and l is half the mould gap width. The values of the constants used in this simulation are listed in Table II.

Table II. Values of the constants used to verify the temperature distribution

Constant	Value
h	1
β	1
u	1
T_0	0
$T_{\text{mould wall}}$	100

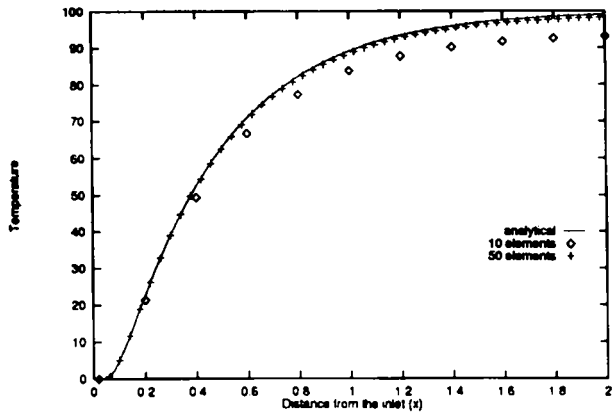

Figure 18. Temperature distribution along the mould mid-plane for two different mesh sizes

The simulation was performed using a number of different mesh sizes. The number of elements in the in-plane direction perpendicular to the flow was kept at three and in the direction of flow 10, 25 and 50 elements were used. Through the thickness three, five and seven control volumes were used. Figure 18 depicts the temperature distribution in the mould mid-plane just after the mould has completely filled for the cases in which the number of elements along the mould was varied and the number of through-thickness control volumes was set to five. For clarity only the results for 10 and 50 elements are plotted. As a reference the theoretical temperature profile is also shown.

The simulation using 10 elements gives errors of more than 6%; however, the largest error for 25 elements is less than 3%. For 50 elements the error is less than 1%.

Figure 19 plots the relative error for the cases in which the number of through-thickness control volumes was varied. In these cases the number of elements along the mould was kept at 25. When using only three control volumes, significant errors of about 10% occur; when five control volumes are used, the error reduces to less than 3%; and for seven control volumes the error is approximately 1%. At the inlet the error is zero, since the temperature at that node is

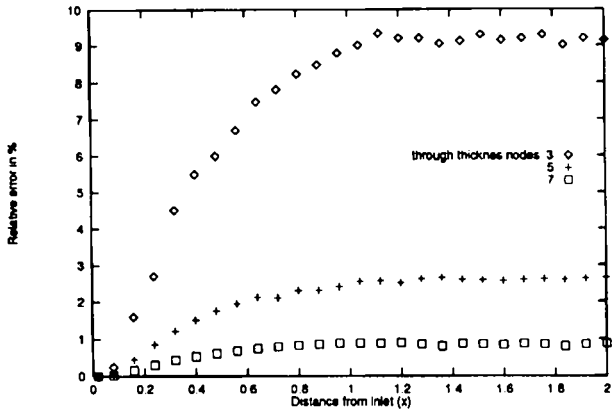

Figure 19. Percentage error in the temperature along the mould mid-plane for a number of different mesh sizes

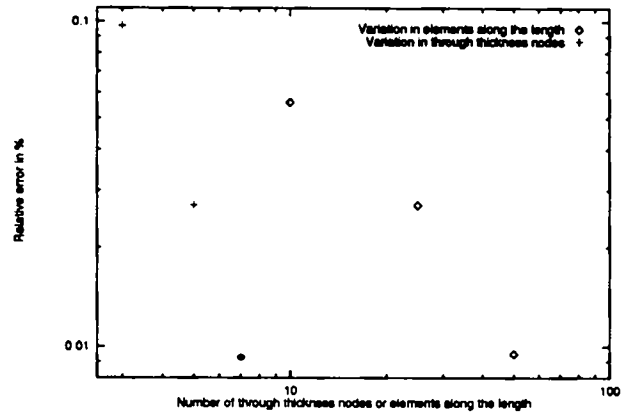

Figure 20. Convergence for refining the mesh through the thickness and in the length directions

specified by the inlet boundary condition. Note that it is computationally more efficient to increase the number of through-thickness nodes than the number of in-plane elements. To achieve an accuracy of 1%, one can either use 50 elements in the length direction and five through-thickness nodes or 25 elements in the length direction and seven through-thickness nodes. In the first case there are 250 temperature nodes; in the second there are only 175 and one only needs to solve for the pressure in half the nodes, resulting in 60% less CPU time. Figure 20 shows the convergence for both types of mesh refinements.

The average number of iterations required to achieve convergence to 10^{-5} was six. As the mould fills slightly, one or two more iterations are required than at the beginning of the mould filling. These results indicate that the numerical implementation does converge to the analytical solution.

4. CASE STUDY

To illustrate the mould filling of a three-dimensional part, we simulated the filling process for the cross-member of a passenger van.[37] Figure 21 shows the finite element discretization of the cross-member. It is a closed thin shell part with a foam core. The part has a complex geometry, including four holes at the bottom. The mesh has approximately 2200 nodes and 2500 elements. Seven through-thickness temperature nodes were used for this simulation. In this case the mould is filled uniformly with random mat. The parameters used in the simulation are listed in Table III.

Figure 22 shows the flow front versus time for the mould-filling simulation. Resin is injected

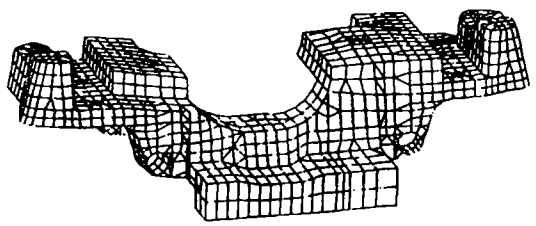

Figure 21. Finite element discretization of a cross-member for a passenger van

Table III. Parameters used in the simulation of the mould filling of a cross-member of a passenger van (partially from References 18 and 26)

Preform properties	
ϕ	0·75
K_{11} (m^{-2})	$1{\cdot}63 \times 10^{-6}$
K_{22} (m^{-2})	$1{\cdot}63 \times 10^{-6}$
Boundary conditions	
P_i (Pa)	5×10^5
T_i (°C)	20
$T_{mould\ wall}$ (°C)	100
C_{hc} (m^{-1})	50
T_g (°C)	80
Thermal properties	
ρ_r (kg m^{-3})	1280
c_{p_r} (J kg^{-1} K^{-1}	1900
ρ_f (kg m^{-3})	2560
c_{p_f} (J kg^{-1} K^{-1})	880
κ_f (W m^{-1} K^{-1})	1·00
κ_r (W m^{-1} K^{-1})	0·2
Kinetic properties	
A_1 (s^{-1})	$1{\cdot}36 \times 10^{28}$
E_1 (kJ mol^{-1})	224·4
A_2 (s^{-1})	$1{\cdot}25 \times 10^{28}$
E_2 (kJ mol^{-1})	223·0
m	0·226
n	1·856
E_α (J g^{-1})	347
Chemorheological properties	
a_0 (N s m^{-2})	$6{\cdot}41 \times 10^{-5}$
b_0	23·1
a (kJ mol^{-1})	32·6
b (kJ mol^{-1})	18·3

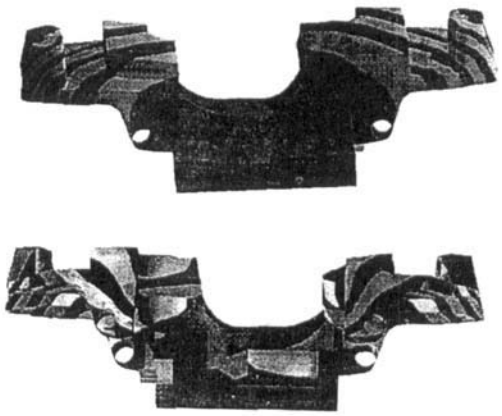

Figure 22. Flow front versus time for the non-isothermal mould filling of a cross-member. Each contour represents 12 s

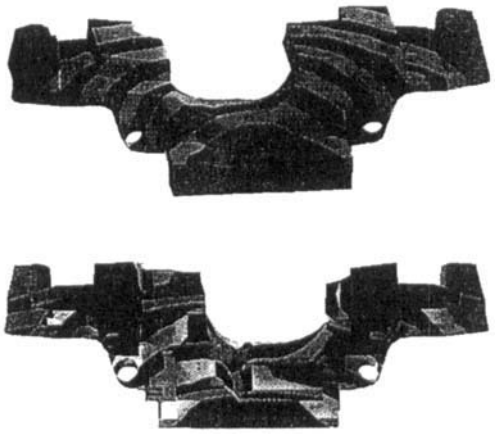

Figure 23. Temperature distribution along the mid-plane of the cross-member of a passenger van. Each contour represents 8 °C

from the centre front. The flow front progresses along the top and bottom of the part and merges at the back. From the results it is clear that one needs exit gates at the top of the mould, at the back centre and at the circular holes to prevent air entrapment in the mould.

Figure 23 shows the temperature distribution along the mould mid-plane when the mould has just filled completely. As expected, the temperature is highest near the top corners of the mould, since that is the area that filled last. The temperature near the inlet is close to the inlet boundary condition. Figure 24 shows the onset of cure at the points where the resin has the longest residence time and the highest temperature, about 2 min after the mould filling has completed. On average about seven to eight iterations were required to achieve convergence to 10^{-4} on the temperature solution.

The results of the simulation were compared with actual flow front positions obtained from short-shot experiments. Good qualitative agreement was found.[36] The deviations between experiments and simulation results are attributed to preform non-uniformities.

The finite element/control volume method is very suitable for handling such geometries. Simulating flow in a complex structure such as this requires no additional numerical techniques. It is worth noting that despite the large and complex mesh, the CPU time is less than 5 h on a Sun 670MP, illustrating that the finite element/control volume method is not CPU-intensive as compared with other numerical techniques.

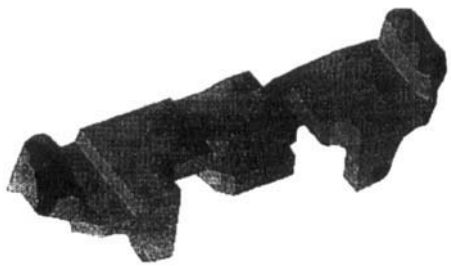

Figure 24. Degree of conversion at the onset of cure in the cross-member of a passenger van. Each contour represents 7% conversion. The maximum degree of conversion is 70%

5. CONCLUSIONS

A numerical simulation was developed to predict the free surface and its interactions with heat transfer and cure for flow of a shear-thinning resin through the fibre preform. The flow part of the simulation is based on the finite element/control volume method. Since the traditional control volume approach produces an error associated with a mass balance inconsistency, a new method was proposed, the element control volume method.

The heat transfer and cure analysis in the simulation are based on the finite difference/control volume method. Since the conduction of heat is important in the through-thickness direction and the convection is important in the plane, the heat transfer and cure are solved in fully three-dimensional form. A simple concept of the boundary condition constant was introduced which models a realistic mould configuration with a heating element located at a distance behind the mould wall. The varying viscosity throughout the mould associated with the temperature and degree of cure distribution is accounted for in calculating the mould-filling pattern. This introduces a two-way coupling between momentum and energy transport in fibrous media.

The simulation was verified by comparing the results with closed form solutions in simple geometries. A case study of a complex three-dimensional part was presented to illustrate the robustness and computational efficiency of the numerical simulation.

REFERENCES

1. M. V. Bruschke and S. G. Advani, 'Flow of generalized Newtonian fluids across a periodic array of cylinders,' *J. Rheol.*, **37**, 479–498 (1993).
2. T. A. K. Sadiq, R. S. Parnas and S. G. Advani, 'Experimental investigation of flow in resin transfer molding,' *Proc. 24th Int. SAMPE Techn. Conf.*, SAMPE, 1992.
3. C. D. Rudd, M. J. Owen, V. Middleton, K. N. Kendall and I. D. Revill, 'Developments in resin transfer moulding for high volume manufacture,' *Proc. ASM/ESD Advanced Composites Conf.*, ASM/ESD, 1990, pp. 301–314.
4. F. C. Robertson, 'Resin transfer moulding of resins–a review,' *Br. Polym. J.*, **20**, 417–429 (1988).
5. C. L. Tucker III and R. B. Dessenberger, 'Governing Equations for Flow and Heat Transfer in Stationary Fiber Beds', in *Flow and Rheology in Composites Manufacturing*, ed. by S.G. Advani, Elsevier, Amsterdam, 1994.
6. M. V. Bruschke, S. G. Advani and R. S. Parnas, 'Resin Transfer Molding', in *Flow and Rheology in Composites Manufacturing*, ed. by S.G. Advani, Elsevier, Amsterdam, 1994.
7. H. Darcy, *Les Fontaines Publiques de la Ville de Dijon*, Dalmont, Paris, 1856.
8. R. A. Greenkorn, *Flow Phenomena in Porous Media*, Marcel Dekker, New York, 1983.
9. M. V. Bruschke and S. G. Advani, 'Mold filling of generalized Newtonian fluids in anisotropic porous media,' in *Transport Phenomena in Material Processing*, ASME Trans. HTD, Vol. 132, 149–158 (1990).
10. M. V. Bruschke and S. G. Advani, 'A finite element/control volume approach to mold filling in anisotropic porous media,' *Polym. Compos.*, **11**, (1990).
11. M. J. Liou, W. B. Young, K. Rupel, K. Han and L. J. Lee, 'Mold filling analysis of resin transfer molding,' *Proc. Fabricating Composites '89*, SME, 1989.
12. F. Trochu, R. Gauvin and Z. Zhang, 'Simulation of mold filling in resin transfer molding by non-conforming finite elements,' *Proc. 3rd Int. Conf. CADCOMP '92*, 1992.
13. F. Trochu and R. Gauvin, 'Limitations of a boundary-fitted finite difference method for the simulation of the resin transfer molding process,' *J. Reinforced Plast. Compos.*, **11**, 772–786 (1992).
14. C. L. Tien, 'Convective and radiative heat transfer in porous media,' *Adv. Appl. Mech.*, **27**, 225–281 (1990).
15. K. Vafai and M. Sozen, 'A comparative analysis of multiphase transport models in porous media,' *Ann. Rev. Heat Transfer*, **3**, 145–162 (1990).
16. S. Whittaker, 'Simultaneous heat, mass and momentum transfer in porous media: a theory of drying,' *Adv. Heat Transfer*, **13**, (1977).
17. D. A. Nield and A. Bejan, *Convection in Porous Media*, Springer, New York, 1992.
18. F. N. Scott, 'Processing characteristics of polyester resin for the resin transfer moulding process,' *Ph.D. Thesis*, University of Nottingham, 1988.
19. R. Lin, L. J. Lee and M. J. Liou, 'Nonisothermal mold filling in resin transfer molding and structural resin injection molding,' *Proc. 49th Ann. Tech. Conf.—ANTEC 91*, SPE, 1991.
20. M. Uenoyama and S. I. Güçeri, 'Analysis and simulation of structural resin injection molding,' *Tech. Rep. 91-09*, Center for Composites Materials, University of Delaware, Newark, DE, 1991.
21. M. J. Owen, V. Middleton, C. D. Rudd, F. N. Scott, K. F. Hutcheon and I. D. Revill, 'Materials behaviour in resin transfer moulding (RTM) for volume manufacture,' *Plast. Rubber Process. Appl.*, **112**, 221–225 (1989).

22. J. L. Whitney and R. L. McCullough, *Delaware Composites Design Encyclopedia*, Vol. 2, *Micromechanical Materials Modeling*, Technomic, Lancaster, 1990.
23. S. Sourour and M. R. Kamal, *SPE Tech. Paper 18(93)*, 1972.
24. M. R. Kamal, S. Sourour and M. Ryan, *SPE Tech. Paper 18(187)*, 1973.
25. M. R. Kamal and S. Sourour, *Polym. Eng. Sci.*, **13**, (1973).
26. D. S. Lee and C. D. Han, 'A chemorheological model for the cure of unsaturated polyester resin,' *Polym. Eng. Sci.*, **27**, 955–963 (1987).
27. T. A. Osswald and C. L. Tucker, *Int. Polym. Process.*, (1990).
28. H. P. Wang and H. S. Lee, 'Numerical techniques for free and moving boundary problems,' in *Fundamentals of Computer Modeling for Polymer Processing*, Hanser, Munich, 1989, pp. 369–399.
29. V. W. Wang, C. A. Heiber and K. K. Wang, *SPE Tech. Paper 31*, 1985.
30. J. P. Coulter, B. F. Smith and S. I. Güçeri, *Proc. 2nd Tech. Conf.*, ASC, 1987, p. 209.
31. C. L. Tucker, *Injection and Compression Molding Fundamentals*, Marcel Dekker, New York, 1987.
32. C. A. Hieber and S. F. Shen, *J. Non-Newtonian Fluid Mech.*, **7**, (1980).
33. P. Virlouvet and C. L. Tucker, 'Volume conserving finite elements for mold filling simulations,' *Proc. Polymer Processing Society 7th Ann. Meet.*, 1991.
34. P. J. Roache, *Computational Fluid Dynamics*, Hermosa, Albuquerque, NM, 1985.
35. C. A. J. Fletcher, *Springer Series in Computational Physics*, Vol. 1, *Computational Techniques for Fluid Dyamics*, 2nd edn, Springer, Berlin, 1990.
36. M. V. Bruschke, 'A predictive model for permeability and non-isothermal flow of viscous and shear-thinning fluids in anisotropic fibrous media,' *Ph.D. Thesis*, University of Delaware, Newark, DE, 1992.
37. C. F. Johnson and N. G. Chavka, 'Preform development for a structural composite crossmember,' *Proc. Fourth Ann. Conf. on Advanced Composites*, ASM International, Metals Park, OH, 1988, pp. 353–365.